Mutations in Citron Kinase Cause Recessive Microlissencephaly with Multinucleated Neurons

Brian N. Harding,[1,12] Amanda Moccia,[2,12] Séverine Drunat,[3,4] Omar Soukarieh,[5] Hélène Tubeuf,[5,6] Lyn S. Chitty,[7] Alain Verloes,[3,4] Pierre Gressens,[4,8,9] Vincent El Ghouzzi,[4] Sylvie Joriot,[10] Ferdinando Di Cunto,[11] Alexandra Martins,[6] Sandrine Passemard,[3,4,8] and Stephanie L. Bielas[2,*]

Primary microcephaly is a neurodevelopmental disorder that is caused by a reduction in brain size as a result of defects in the proliferation of neural progenitor cells during development. Mutations in genes encoding proteins that localize to the mitotic spindle and centrosomes have been implicated in the pathogenicity of primary microcephaly. In contrast, the contractile ring and midbody required for cytokinesis, the final stage of mitosis, have not previously been implicated by human genetics in the molecular mechanisms of this phenotype. Citron kinase (CIT) is a multi-domain protein that localizes to the cleavage furrow and midbody of mitotic cells, where it is required for the completion of cytokinesis. Rodent models of *Cit* deficiency highlighted the role of this gene in neurogenesis and microcephaly over a decade ago. Here, we identify recessively inherited pathogenic variants in *CIT* as the genetic basis of severe microcephaly and neonatal death. We present postmortem data showing that CIT is critical to building a normally sized human brain. Consistent with cytokinesis defects attributed to CIT, multinucleated neurons were observed throughout the cerebral cortex and cerebellum of an affected proband, expanding our understanding of mechanisms attributed to primary microcephaly.

Primary microcephaly is a genetically heterogeneous neurodevelopmental disorder characterized by a severe reduction in brain growth.[1] This decreased brain volume often stems from a primary defect in neurogenesis. The cerebral cortex is composed of neurons born from neural progenitor cells (NPCs) that reside adjacent to the lateral ventricle during early neurodevelopment.[2] The mitotic machinery of NPCs is critical for rapid expansion of the progenitor pool underlying normal brain growth and maintenance of neural progenitor multipotency. Largely on the basis of human genetic findings, primary microcephaly has been attributed to defects in the fidelity of mitotic-spindle placement and centrosome stability.[3–8] Surprisingly, other steps in mitosis have not been implicated by neurogenetics in the pathophysiology of microcephaly, despite a series of rodent models showing that cleavage-furrow placement, constriction of the contractile ring, and abscission by the midbody are critical for neurogenesis.[9–11]

Citron kinase (CIT) is a multi-domain protein that localizes to the cleavage furrow and midbody, where it functions in cytokinesis, the final step of mitosis (Figure 1A).[12,13] CIT has an N-terminal kinase domain and a number of C-terminal domains that facilitate interactions between components of the contractile ring (anillin, actin, myosin, and RhoA). Although the endogenous substrates of CIT have yet to be confirmed, experimental data from multiple organisms have shown that the kinase activity and scaffolding functions of this protein are both important for successful completion of cytokinesis.[12,14,15] Conversely, neurons with two or more fully formed nuclei can result from incomplete cytokinesis. The impact of cytokinesis defects on brain development and size are evident in the *Cit* knockout mouse and the *Flathead* rat, which has a spontaneous nonsense mutation in *Cit* exon 1. In rodents, CIT is critical for the proliferation of NPCs and male germ cell precursors. *Cit*-null animals are characterized by microcephaly, testicular hypoplasia, ataxia, growth deficiencies, and lethal seizures.[10,11] These phenotypes have been linked to cytokinesis defects and the presence of multinucleated cells throughout the cortex and cerebellum. Premature differentiation of early NPCs and widespread apoptosis accumulate across development, resulting in a cerebral cortex and cerebellum less than 50% of the size of a normal brain. Cortical hypoplasia and layer disorganization are predicted to account for the recurrent spontaneous seizures and premature death in these mice.[16] Roles for *CIT* (MIM: 605629) in human brain development and primary microcephaly have been predicted but not yet reported.

Here, we describe three independent families (A, B, and C) each with multiple affected children who present with severe microlissencephaly associated with neonatal mortality (Figure 1B). The clinical features of the probands are provided in Table 1. Egyptian family A

[1]Pathology and Laboratory Medicine, Perelman School of Medicine, University of Pennsylvania and Children's Hospital of Philadelphia, Philadelphia, PA 19104, USA; [2]Department of Human Genetics, University of Michigan Medical School, Ann Arbor, MI 48109, USA; [3]Département de Génétique, Protect, Hôpital Robert Debré, Paris 75019, France; [4]INSERM U1141, Hôpital Robert Debré, Paris 75019, France; [5]INSERM U1079, Institute for Research and Innovation in Biomedicine, University of Rouen, Normandy Centre for Genomic and Personalized Medicine, Rouen 76183, France; [6]Interactive Biosoftware, Rouen 76000, France; [7]Genetics and Genomic Medicine, UCL Institute of Child Health and Great Ormond Street NHS Foundation Trust, London WC1N 1EH, UK; [8]Université Paris Diderot, Hôpital Robert Debré, Paris 75019, France; [9]Center for Developing Brain, King's College, St. Thomas' Campus, London WC2R 2LS, UK; [10]Service de Neuropédiatrie, Centre Hospitalier Régional Universitaire de Lille, Lille 59037, France; [11]Department of Molecular Biotechnology and Health Sciences, University of Turin, Turin 10126, Italy
[12]These authors contributed equally to this work
*Correspondence: sbielas@umich.edu
http://dx.doi.org/10.1016/j.ajhg.2016.07.003.

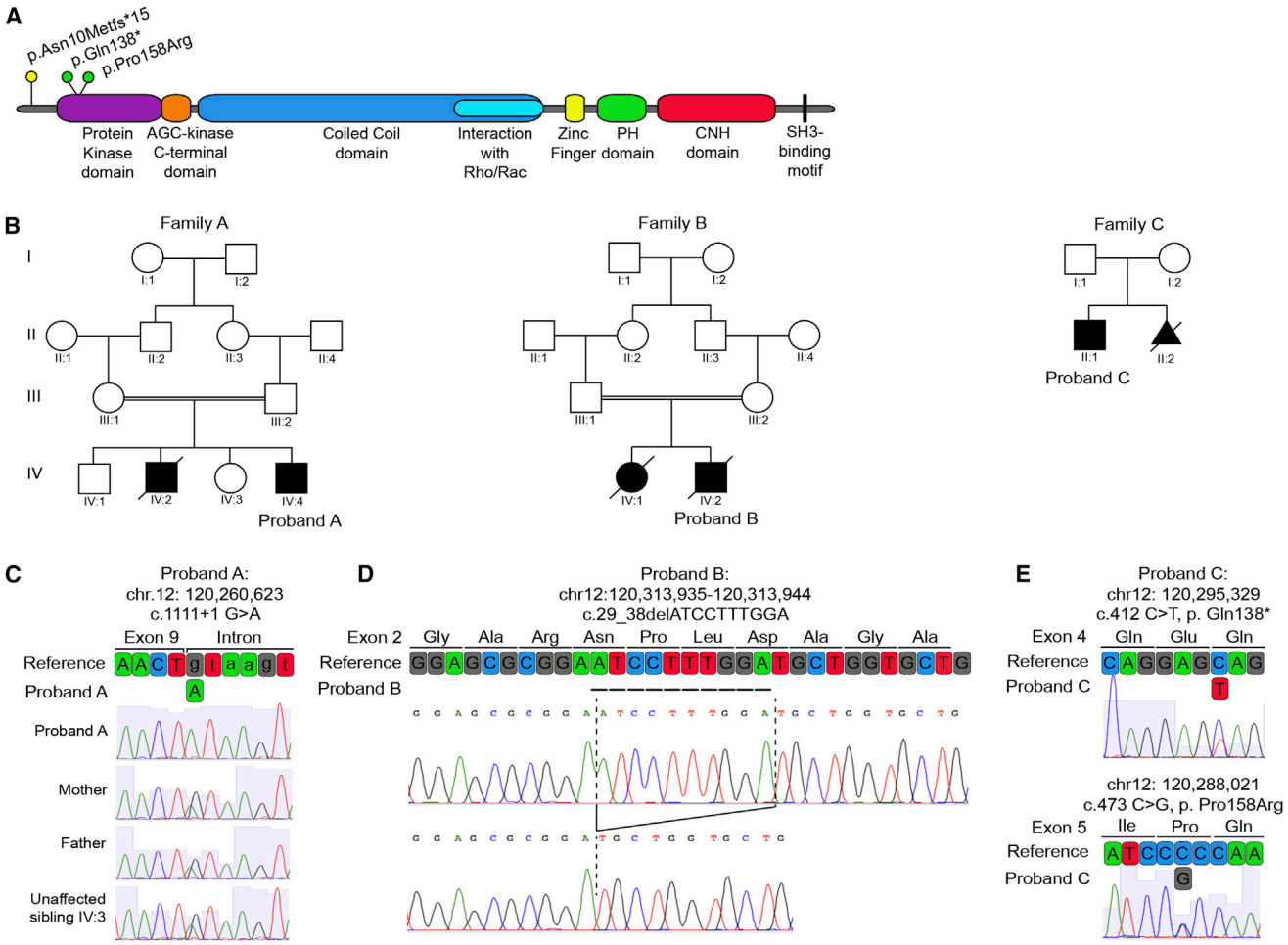

Figure 1. Recessive *CIT* Variants in Microlissencephaly
(A) Domain organization of CIT shows pathogenic coding variants in relation to protein domains.
(B) Pedigrees of the families investigated; probands are noted.
(C) Chromatographs and schematic of the boundary between exon 9 and intron 9 of WT reference *CIT*, the homozygous splice donor variant from proband A (c.1111+1G>A), and the cryptic splice donor site four bases downstream. Parents and unaffected sibling IV:3 are heterozygous carriers.
(D) Chromatographs defining the homozygous 10 bp *CIT* exon 2 deletion (c.29_38delATCCTTTGGA; hg19 chr12: 120,313,935–120,313,944) amplified from proband B. This deletion creates a frameshift leading to a premature stop 15 codons downstream (not shown).
(E) Chromatographs and schematic of reference *CIT* exons 4 and 5 and the corresponding nonsense (c.412C>T [p.Gln138*]) and missense (c.473C>G [p.Pro158Arg]) variants identified in proband C.

is consanguineous with two microcephalic male siblings. The first affected child died in the neonatal period (Figure 1B). Proband A was delivered at term and weighed 2,600 g (2 SDs below the age and sex mean), consistent with the fifth percentile for growth. Head circumference, not measured until 3.5 months of age, was 27 cm (11–12 SDs below the age and sex mean). His length at 3.5 months was 53 cm (4–5 SDs below the age and sex mean), and he continued to experience failure to thrive thereafter. Dysmorphisms included hypotelorism, a sloping forehead, and relatively large ears (Figure 2A). He exhibited axial hypotonia, hypertonia of the upper and lower extremities, increased deep tendon reflexes, and a lack of head support. Microcephaly was confirmed by MRI, which revealed lissencephaly, enlarged ventricles, agenesis of the corpus callosum, cerebellar hypoplasia, and brainstem hypoplasia (Figure 2B). T2 hyperintensity was also noted throughout the white matter, consistent with spastic tetraplegia.

Family B has two affected children born to consanguineous parents from the United Arab Emirates. Male proband B was noted to have microcephaly, intrauterine growth retardation, and oligohydramnios by ultrasound at 30 gestational weeks (GWs). Echocardiography indicated cardiomegaly, biventricular dilatation, and tricuspid regurgitation. He was delivered by spontaneous vaginal delivery at 39 GWs with a head circumference of 24 cm (8 SDs below the age and sex mean) and a body length of 27.2 cm from crown to rump (2.5 SDs below the mean), consistent with 36 GWs. Despite Apgar scores of 8 at 1 min and 9 at 5 min, he died the following day.

At birth, the brain weight of proband B was 40 g (10% of the average newborn brain weight of 390 g). The cerebral

Table 1. Genetic and Major Clinical Features

	Proband A	Proband B	Proband C	Subject II:2 of Family C
CIT variant (hg19, GenBank: NM_007174.2)	chr12: 120,260,623	chr12: 120,313,935–120,313,944	chr12: 120,295,329 and chr12: 120,288,021	chr12: 120,295,329 and chr12: 120,288,021
	c.1111+1G>A	c.29_38delATCCTTTGGA	c.412C>T and c.473C>G	c.412C>T and c.473C>G
	–	p.Asn10Metfs*15	p.Gln138* and p.Pro158Arg	p.Gln138* and p.Pro158Arg
GERP score	5.900	NA	4.660 and 5.280	4.660 and 5.280
CADD score	31.000	NA	38.000 and 27.800	38.000 and 27.800
Gender	male	male	male	male
Gestational length	full term	full term	full term	pregnancy terminated at GW 29 + 2
Birth weight	2.6 kg (−2 SDs)	1.730 kg (−4 SDs)	2.92 kg (−1 SD)	NA
Birth length	unknown (home birth)	27.2 cm crown to rump (−2.5 SD)	46 cm (−2 SDs)	NA
Birth head circumference	unknown (home birth)	24 cm (−8 SDs)	30 cm (−3.5 SDs)	NA
Head circumference at most recent evaluation	27 cm (−11 to −12 SDs) measured at 3.5 months	NA	43 cm (−6.5 SDs) measured at 10 years	NA
Brain abnormalities	MRI revealed microlissencephaly, agenesis of corpus callosum, cerebellar and brainstem hypoplasia, and T2 hyperintensity of the whole white matter	autopsy revealed microlissencephaly, absent corpus callosum, hindbrain and cerebellum hypoplasia, cerebral cortex hypoplasia, and comparatively large ventricles; a detailed neuropathology is included in the main text	MRI revealed microcephaly, a simplified gyral pattern, and cerebellar and brainstem hypoplasia	fetal MRI revealed microcephaly, a biparietal diameter equivalent to that of a fetus of 23 GWs, and gyration equivalent to a that of a fetus of 26 GWs
Neurological findings	hypertonia of upper and lower extremities, axial hypotonia, increased DTRs, and spastic tetraplegia	NA	hypertonia of upper and lower extremities and brisk DTRs in the lower extremities	NA
Seizures	no	NA	no	NA
Intellectual disability	not assessed	NA	moderate to severe ID with mild autistic features	NA
Development	delayed	NA	delayed	NA
Dysmorphisms	hypotelorism, sloping forehead, and relatively large ears	prominent occiput, absent fontanelle, large ears, wide nasal bridge, prominent upper lip, high-arched palate, cloudy corneas, right-sided single palmar crease, and small nails	sloping forehead, prominent nose, and relatively large ears	NA
Status	unknown	died 1 day after birth	alive	terminated pregnancy

World Health Organization Child Growth Standards were applied for weight, height, and head circumference. Abbreviations are as follows: DTR, deep tendon reflex; GW, gestational week; and NA, not available.

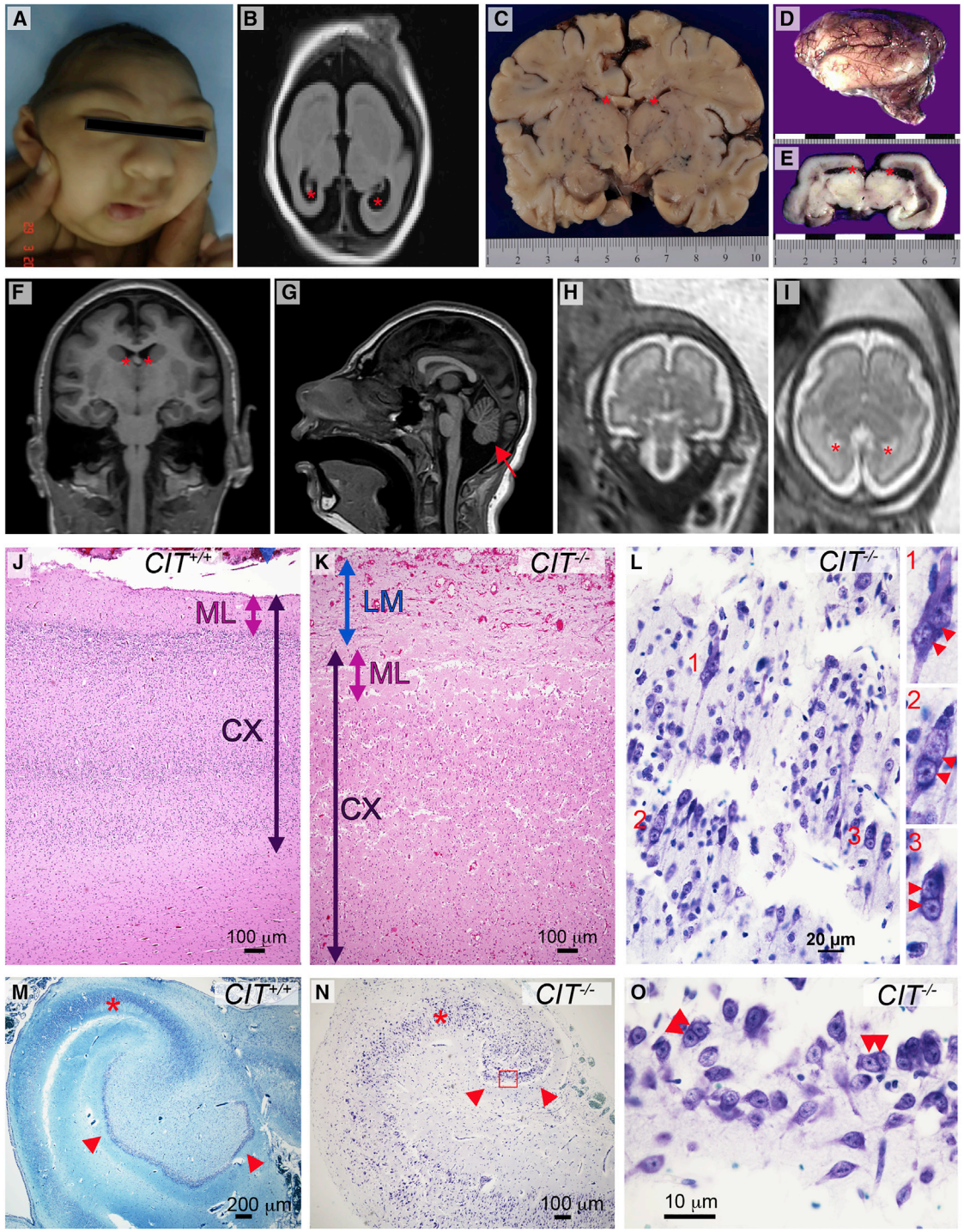

Figure 2. Structural and Cellular Neocortical Phenotypes

(A) Proband A displays a microcephalic cranium, a sloping forehead, a wide nasal bridge, and hypotelorism.

(B) T2-weighted axial MRI of proband A at 3.5 months shows markedly reduced cerebral cortical size, simplified gyral folding, and enlarged ventricles (red asterisks).

(C) Coronal section of newborn control brain. Width is in centimeters, and lateral ventricles are marked by red asterisks.

(D) Lateral view of the lissencephalic newborn brain from proband B (scale in centimeters).

(E) Coronal section through the mid-thalamus of the brain of proband B shows enlarged lateral ventricles (red asterisks).

(F) Coronal brain MRI of proband C at 10 years of age shows microcephaly, a simplified gyral pattern, and enlarged ventricles (red asterisks).

(G) Mid-sagittal MRI of proband C shows a sloping forehead and a hypoplastic brainstem and cerebellum (red arrow).

(H and I) Coronal (H) and axial (I) fetal brain MRI of affected subject C:II:2 at 29 GWs shows reduced brain volume, reduced gyrification, and enlarged ventricles (red asterisks).

(legend continued on next page)

hemispheres were lissencephalic apart from shallow Sylvian fissures. Large ventricles, small well-delineated basal ganglia and thalami, and agenesis of the corpus callosum were noted (Figures 2C–2E). The brain stem and cerebellum were hypoplastic with small cerebellar folia (Figure 4A). Dysmorphic facial features included a prominent occiput, an absent fontanelle, large ears, a wide nasal bridge, a prominent upper lip, a highly arched palate, cloudy corneas, a right-sided single palmar crease, and hypoplastic nails. Renal aplasia was also noted. These features were similar to those observed during the pregnancy and birth of an affected female sibling who presented with microcephaly and renal agenesis and survived only 4 hr after birth (Figure 1B).

Proband C is the first-born son of unrelated French parents and was delivered at full term. His birth weight was 2,900 g, his body length was 46 cm, and his head circumference was 30 cm (1, 2, and 3.5 SDs below the age and sex mean, respectively), consistent with a diagnosis of microcephaly. Proband C presented with a sloping forehead, a prominent nose, and relatively large ears. His neurological examination was remarkable for hypertonia of the upper and lower limbs and brisk tendon reflexes in the lower limbs. He walked independently at 18 months of age. He has developmental delay with moderate to severe ID and mild autistic features. No metabolic, electroretinographic, or electroencephalographic abnormalities were detected. By the age of 10 years, his head circumference was 6.5 SDs below the age and sex mean. MRI performed at this age showed a simplified gyral pattern and a hypoplastic cerebellum (Figures 2F and 2G). A second child in this family (II:2) was also confirmed to have microcephaly by fetal MRI at 29 GWs (Figures 2H and 2I). The biparietal diameter measured from the fetal MRI at that time was consistent with 23 GWs.

Although the microcephalic phenotype displayed by these probands aligns with a diagnosis of autosomal-recessive primary microcephaly (MCPH [MIM: 251200]), the additional syndromic features and neonatal mortality suggest that this is not classic MCPH. In order to identify a genetic diagnosis for these three probands, we employed whole-exome sequencing (WES) and candidate gene screening. Parents provided written informed consent that was approved by institutional review boards at the respective institutions. Quad WES (mother, father, proband, and unaffected sibling) was performed for family A to identify pathogenic variants. DNA was isolated from peripheral blood according to standard procedures. WES was performed at the Beijing Genomics Institute (BGI) according to standard protocols for Agilent SureSelect All Exon Kit V4 library preparation and Illumina HiSeq 2000 sequencing to a mean sequence depth of 98× for 99% exome coverage, and the sequence was analyzed with the SOAPaligner.[17,18] Variants were filtered against dbSNP, 1000 Genomes, the NHLBI Exome Sequencing Project (ESP) Exome Variant Server (ESP6500), and the BGI SNP database. An average of 65,457 high-quality single-nucleotide variants and indels were identified per individual. Common variants (with a minor allele frequency [MAF] > 0.005) were removed, and rare variants were analyzed in relation to homozygous recessive, compound-heterozygous, and dominant modes of inheritance. Targeted analysis did not identify a causal mutation in any gene present in the OMIM database and was therefore followed by a complete analysis of all coding regions. A homozygous recessive G>A transition (c.1111+1G>A [GenBank: NM_007174.2]; hg19 chr12: 120,260,623) disrupting the donor splice site (5′ ss) of exon 9 in *CIT* was identified, consistent with consanguinity (Figure 1C). Segregation of this variant in the family was confirmed by Sanger sequencing, and both parents and the unaffected sibling were found to be heterozygous carriers.

The c.1111+1G>A variant's potential impact on RNA splicing was first evaluated by in silico approaches (Human Splicing Finder and MaxEntScan). This analysis predicted the destruction of the reference 5′ ss and revealed the presence of cryptic donor sites both upstream and downstream (Figure 3A). We evaluated the impact on splicing experimentally by performing a minigene reporter assay as previously described.[19] We amplified the genomic region of interest (*CIT* exon 9 and at least 150 bp of flanking intronic sequences) from control and proband A (*CIT* c.1111+1G>A) genomic DNA and cloned it into the intron of the pCAS2 reporter plasmid to generate three-exon wild-type (WT) and mutant minigenes, respectively. Plasmids were transfected into HeLa cells, RNA was extracted 24 hr after transfection, and the splicing pattern of the minigenes was assessed by RT-PCR and sequencing of the gel-purified RT-PCR products.[20] Our results confirmed that the c.1111+1G>A variant results in the production of aberrantly spliced transcripts as a result of the concomitant destruction of the reference 5′ ss and activation of two cryptic splice sites located nearby. The major aberrant transcripts induced by c.1111+1G>A result from activation of a cryptic splice site located downstream of the reference 5′ ss, leading to the aberrant retention of four nucleotides from intron 9 in the minigene's

(J and K) Control (J) and proband B (K) cerebral cortex stained with H&E. Compared to the control, leptomeninges (LM; blue arrow) in the proband are excessively thick and contiguous with the molecular layer (ML; pink arrow). Compared to the control, the proband's cortex (CX; dark purple arrow) is thickened, and the cortical layering is obscure.
(L) High magnification of proband B cortex stained with Kluver-Barrera. Disorganized parenchyma includes many multinucleated neurons: inserts show detail of multinucleated (red double arrowheads) cells labeled 1, 2, and 3.
(M and N) Kluver-Barrera-stained sections of control (M) and proband B (N) temporal lobe. The proband hippocampus is very small and has a hypoplastic pyramidal layer (red asterisk) and greatly reduced dentate gyrus (arrowheads). The normal control hippocampus was imaged at half the magnification to allow for a comparison of the overall hippocampal structure.
(O) Detail of the dentate gyrus from proband B (red box in N) shows binucleated granule cells (double arrowheads).

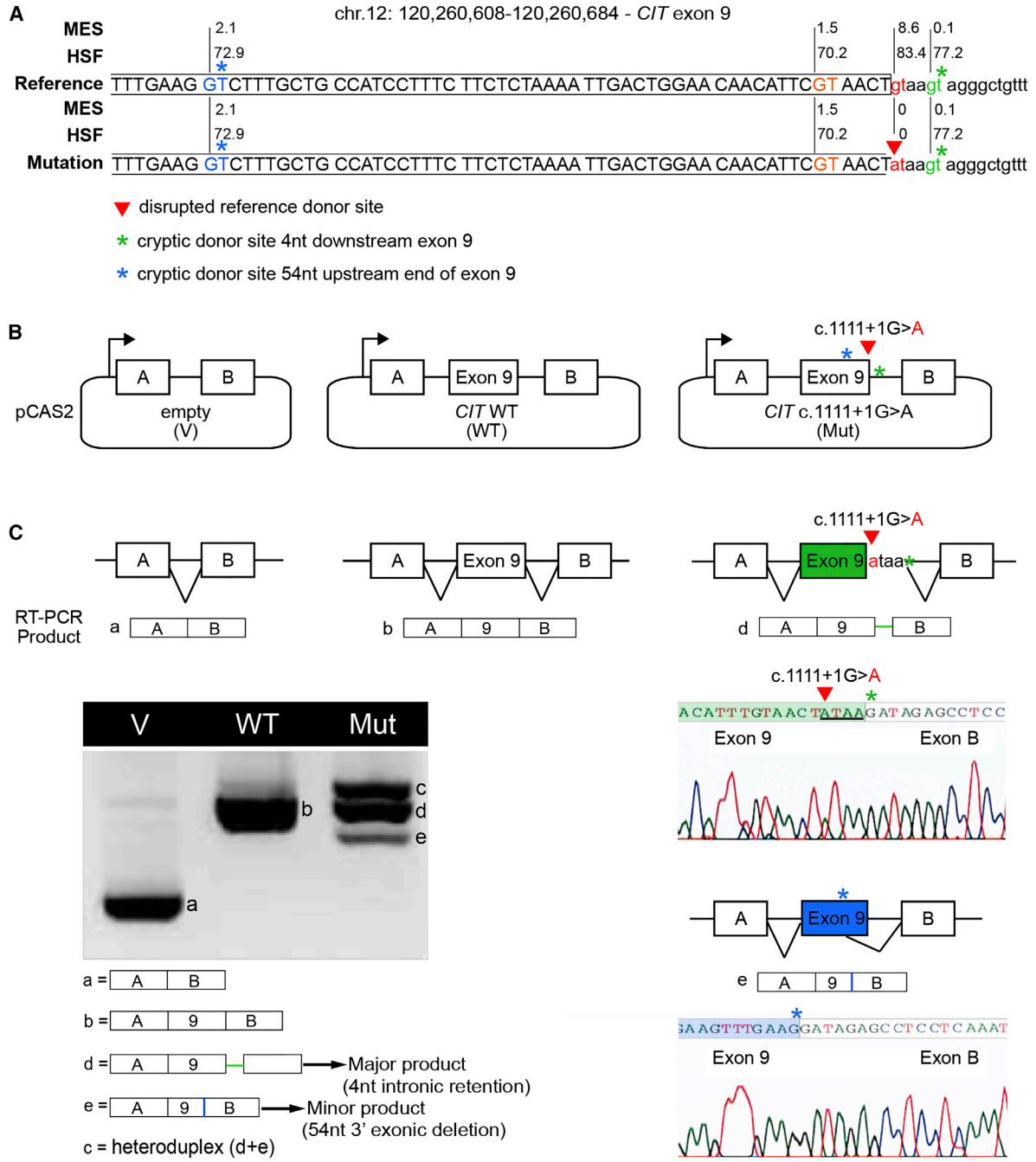

Figure 3. Functional Analysis of *CIT* c.1111+1G>A Confirms Its Negative Impact on RNA Splicing
(A) Schematic representation of *CIT* sequence across the boundary between exon 9 and intron 9. The reference donor site (WT, red nucleotides) and cryptic donor sites (blue, orange, and green nucleotides) were delineated and scored with MaxEntScan (MES) and Human Splicing Finder (HSF) as shown in Figure S1. Only splice sites predicted by both algorithms in the WT sequence are shown. Exonic and intronic sequences are indicated by upper and lower case, respectively. The *CIT* c.1111+1G>A mutation from proband A (red arrowhead) disrupts the WT donor site. Asterisks indicate cryptic splice sites activated in the presence of c.1111+1G>A.
(B) A minigene splicing assay was performed as previously described. The structures of the *CIT* exon 9 minigenes were used in the splicing reporter assay. Arrows represent the CMV promoter. Boxes represent exons, and lines in between indicate introns.
(C) Analysis of WT and mutant (Mut) minigene splicing patterns. Transcripts were analyzed by RT-PCR after expression in HeLa cells with the use of primers specific to the minigene's exons A and B (Table S1). RT-PCR products were separated on an agarose gel and sequenced. Aberrantly spliced products, accompanied by chromatographs, are illustrated on the right.

transcripts (Figures 3B–3C and Figure S1). This alteration is expected to introduce a premature stop codon in exon 10 of *CIT*, creating a transcript that is predicted to undergo nonsense-mediated decay. The minor aberrant transcripts induced by c.1111+1G>A result from the activation of a cryptic splice site located upstream of the reference 5′ ss, leading to the aberrant deletion of 54 nucleotides from exon 9 in the minigene's transcripts. This alteration is

expected to produce an in-frame deletion of 18 amino acids in the kinase domain of CIT (CIT^{-18aa}). The stability of mutant CIT^{-18aa} has not been evaluated, but it is possible that the deletion disrupts kinase activity.

Resequencing of *CIT* coding exons and splice junctions in 35 additional probands with primary microcephaly identified two additional individuals, probands B and C, with recessive pathogenic variants. Proband B DNA was extracted from formalin-fixed, paraffin-embedded brain tissue with the QIAGEN QIAamp DNA FFPE Tissue Kit (catalog no. 56404) per the manufacturer's instructions. The 46 coding exons of *CIT* on chromosome 12 were screened by dideoxy sequence analysis on an ABI 3730 sequencer (Applied Biosystems, Life Technologies), and sequence traces were analyzed with Sequencher 5.1 (Gene Codes Corporation). A homozygous pathogenic mutation consistent with consanguinity was identified in proband B. This 10 bp deletion in exon 2 of *CIT* creates a premature stop codon 15 codons downstream (c.29_38delATCCTTTGGA [p.Asn10Metfs*15] [GenBank: NM_007174.2]; hg19 chr12: 120,313,935–120,313,944) and is predicted to function as a null allele (Figures 1A and 1D).

DNA from proband C and subject C:II:2 was isolated from peripheral blood according to standard procedures at the Robert Debré Hospital in Paris. *CIT* was included on a microcephaly gene panel for cohort screening by RainDance microdroplet PCR and 2 × 150 bp sequencing with an Illumina MiSeq system. Deep (142×) sequencing reads were mapped to the UCSC Genome Browser (hg19) with MiSeq analysis software, the Burrows-Wheeler Aligner, and the Genome Analysis Toolkit, and panel exons were 99% covered. Variants were filtered against MAF (>0.005), dbSNP, 1000 Genomes, the NHLBI ESP Exome Variant Server, and an in-house dataset. Rare variants were annotated for functional features of coding nucleotides with publically available databases outlined for WES. Both proband C and subject C:II:2 were found to carry compound-heterozygous *CIT* variants—one generating a nonsense variant in exon 4 (c.412C>T [p.Gln138*]; hg19 chr12: 120,295,329) and the other generating a missense variant in exon 5 (c.473C>G [p.Pro158Arg]; hg19 chr12: 120,288,021), which encodes the kinase domain (Figures 1A and 1E). The *CIT* variants identified in proband B, proband C, and subject C:II:2 (c.29_38delATCCTTTGGA, c.412C>T, and c.473C>G, respectively) did not alter splicing (Figure S1). The p.Pro158Arg (c.473C>G) variant is predicted to disrupt kinase function, but not CIT accumulation. Compared with the homozygous null phenotypes in probands A and B, the severity of the microcephaly exhibited by proband C might be ameliorated by the accumulation of the p.Pro158Arg variant. The parents and unaffected relatives in families B and C were not available for carrier testing.

The *CIT* mutations presented here were absent from online genomic variant databases, including 1000 Genomes, the NHLBI ESP Exome Variant Server, dbSNP 141, and the Exome Aggregation Consortium (ExAC) Browser.[21–23] Bioinformatic variant annotation by SeattleSeq Variation Annotation revealed that the point mutations in our probands affect highly conserved bases with high GERP and CADD scores that are predicted to be pathogenic (Table 1).[24,25] Further analysis of the genetic variation in *CIT* showed that loss-of-function alleles are infrequent. Homozygous nonsense or frameshift variants were not present in the ExAC Browser. However, 15 rare heterozygous truncating variants were detected (MAF < 0.001), suggesting that there is high evolutionary pressure against these alleles and supporting the deleteriousness of the recessive *CIT* variants described here. These findings correspond to a Residual Variation Intolerance Score (RVIS) of −2.35, indicating that *CIT* is in the top 1.14% of genes intolerant to common functional genetic variation.[26]

The cytokinesis functions of CIT have been conserved across evolution. Deficiencies of rodent CIT have been shown to disrupt NPC proliferation, implicating CIT in primary microcephaly. Although severe reductions in brain size are often accompanied by a simplified gyral pattern, gene mutations that disrupt neuronal migration are generally attributed to classical lissencephaly or smooth-brain disorders.[1,27–29] This combination of extreme reduction in brain volume and lissencephaly observed in probands A and B could provide evidence for a reduction in cortical surface area, which does not support gyri formation in the human brain. This idea is supported by the genotypic-phenotypic spectrum of microcephaly to microlissencephaly on the basis of recessive inheritance of *CIT* pathogenic variants, described here and in an accompanying study.[30] Homozygous missense variants in the kinase domain encoded by *CIT* are associated with primary microcephaly with a simplified gyral pattern and few additional syndromic features. Conversely, homozygous null variants in *CIT* represent the severe end of the spectrum associated with extremely small lissencephalic brains and neonatal mortality.

Given the well-established role of CIT in cytokinesis, our three affected individuals provide evidence that this is an important pathogenic mechanism for microcephaly, a disorder previously linked primarily to gene products that localize to the centrosome or mitotic spindle.[31] This cell biology was originally implicated by studies of ASPM, which localizes to the midbody, where it can be co-immunoprecipitated with CIT.[32–34] Severe microcephaly with widespread multinucleated neurons is characteristic of the structural and cellular pathology observed in the *Cit* knockout mouse and the *Flathead* rat (Table S2).[10,11] In accordance with approval by institutional research boards and ethics committees, post-mortem analysis of proband B allowed the human cell and molecular neuropathology associated with pathogenic variants in *CIT* to be analyzed. All non-neural tissue examined had normal cytology, but multinucleated neurons were observed throughout the neuraxis of proband B, a hallmark of cytokinesis defects (Table S3). This neural-specific phenotype is phenocopied in the rodent models, yet the molecular details that underlie the tissue specificity of this feature have not been determined.

To analyze the cytoarchitechture, we stained brain sections from proband B with H&E and stained selected

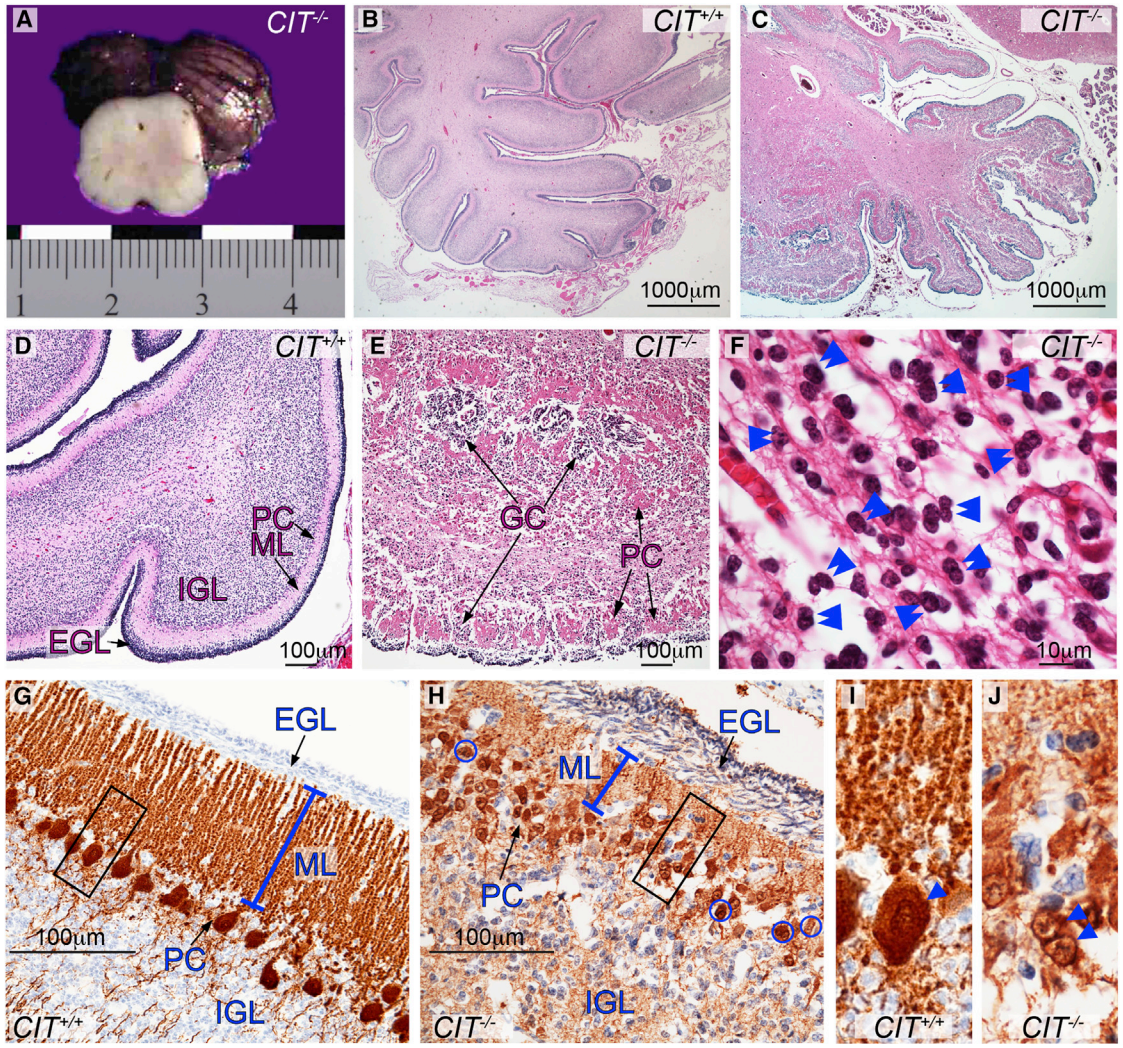

Figure 4. Structural and Cellular Cerebellar *CIT* Phenotypes
(A) Section through the proband B midbrain shows an external view of the hypoplastic cerebellum. The scale is measured in centimeters. (B–F) Histologic cerebellar sections stained with H&E. In proband B, the cerebellar folia are poorly developed and the cortex is disorganized (C, E, and H). Compared to control cerebellum (B and D), cerebellar lamination in proband B is disrupted by clustered Purkinje cells (PCs) interspersed with granule cells (GCs) within fused folia (C and E). Many GCs appear binucleated (F; double blue arrowheads). (G–J) Cerebellum immunostained for calbindin shows that compared to the control (G), proband B has an abnormally thick EGL, a reduced ML (blue line), and multilayered collections of small PCs (H, arrows). The black boxes is (G) and (H) are enlarged to show that compared to control cells (I), PCs from proband B (J, blue arrowheads) are binucleated within a small soma. Abbreviations are as follows: EGL, external granule layer; IGL, internal granule layer; and ML, molecular layer.

sections with Kluver-Barrera or calbindin. Microscopically, the profoundly microcephalic cerebral cortex showed both cytological and organizational abnormalities in many areas. The neocortex was excessively thick, and the six cortical layers were replaced by a molecular layer and two broad layers composed of loosely and irregularly scattered neurons (Figures 2J and 2K). The underlying white matter was unmyelinated and contained scattered ectopic neurons. The overlying leptomeninges were greatly thickened with reticulin and collagen fibers, were prominently vascularized, and contained heterotopic astrocytes and neurons, some of which were multinucleated (Figure 2L). The hippocampi were dysplastic, small, and under-rotated and showed hypoplastic dentate gyri (Figures 2M–2O). These cortical and hippocampal phenotypes are consistent with those observed in rodent models that have been attributed to massive apoptosis during neurodevelopment.[11,16,35] Alternatively, although migration defects have not been described in association with *Cit* mutations in rodents, defective radial migration of human binucleated immature neurons is a novel, as yet untested explanation for this cortical disorganization.

Cortical hypoplasia and layer disorganization account for the recurrent spontaneous seizures associated with premature death in rodent models.[16,35] Extrapolating from these rodent models, the cytoarchitectural abnormalities observed in proband B are consistent with cytokinesis defects that contribute to reduced neuronal precursor proliferation, multinucleation of neurons, and increased cell death. Despite the cytoarchitectural similarities,

pathogenic *CIT* variants have not been detected in epilepsy cohorts, including the Epi4K exome sequence collection of 264 epileptic encephalopathy trios.[36]

Neuropathology studies also revealed that the cerebellar cortex of proband B was hypoplastic and dysplastic (Figure 4). Laminar disorganization was more evident in the hemispheres than the vermis, where folia were fused and Purkinje cells were observed in multilayered islands interspersed with abnormal granule cell domains (Figures 4B–4H). At birth, the external granule cell layer (EGL) is usually compact with four to six rows of bipolar cells abutting the molecular layer (ML) (Figures 4B, 4D, and 4G). In proband B, the EGL was wider, the ML was narrower, and both were merged with the Purkinje cell layer (Figures 4G and 4H). In this case, the EGL was composed of two or three compact rows of cells overlying a looser band of horizontally oriented, thin, elongated cell bodies, some of which were clearly binucleated (Figures 4E, 4F, and 4H). Compared to control cells, Purkinje cells had short simplified dendritic arborization, and many were multinucleated (Figures 4G–4J). Likewise, the internal granular layer was severely hypo-cellular (Figures 4G and 4H).

In summary, we report the identification of pathogenic variants in *CIT* as a genetic basis for primary microcephaly, microlissencephaly, and cerebellar hypoplasia, whose phenotypic features are remarkably similar to those of $Cit^{-/-}$ rodent models. These findings highlight the evolutionarily conserved function of CIT in neurodevelopment and the disproportionate sensitivity of the neuraxis to pathogenic variants in this gene. Alternatively, the differences between non-neural phenotypes observed in proband B and the $Cit^{-/-}$ rodent models might represent the spectrum of species-specific tissues sensitive to homozygous truncating mutations in *CIT* (Table S2). Multinucleated neurons are rarely observed in the nervous system, apart from their occurrence in ganglion cell tumors. These genetic findings implicate novel mechanisms in the pathogenesis of primary microcephaly and allow us to describe the human presentation of this striking multinucleated neuronal phenotype.

Accession Numbers

The accession number for the c.29_38delATCCTTTGGA (chr12: 120,313,935–120,313,944) sequence reported in this paper is ClinVar: SCV000257393. The accession numbers for the *CIT* variants reported in this paper are ClinVar: SCV000257393, SCV000292379, SCV000292380, and SCV000292381.

Supplemental Data

Supplemental Data include two figures and three tables and can be found with this article online at http://dx.doi.org/10.1016/j.ajhg.2016.07.003.

Acknowledgments

We thank the families for their participation and contribution to this research. We appreciate Ritesh K.C. and Brian McGrath for stimulating discussion during manuscript preparation and Dr. Joseph Loturco, Dr. Joseph Gleeson, Dr. Ozgur Rosti, and Dr. Hongda Li for collaborations on *CIT* genetics and molecular biology. This work was supported by the NIH (R00HD069624 to S.L.B), the French Institut National du Cancer and Direction Générale de l'Offre de Soins (AAP/CFB/CI to A.M.), the French Ministry of Education (PhD fellowship to O.S.), the French Association Nationale de la Recherche et de la Technologie in the context of public-private partnership between INSERM and Interactive Biosoftware (CIFRE PhD fellowship to H.T.), and the Programme Hospitalizer de Recherché Clinique (grant no. P100128/IDRCB: 2010-A01481-38) and ERA-NET E-Rare-2 2013 (grant no. ANR-13-RARE-0007-01 2013) to S.D., A.V., V.E.G., P.G., and S.P. The sponsors of the study had no role in study design, data collection, analysis and interpretation, or writing of the manuscript.

Received: April 27, 2016
Accepted: July 5, 2016
Published: July 21, 2016

Web Resources

1000 Genomes Project, http://browser.1000genomes.org
ClinVar, http://www.ncbi.nlm.nih.gov/clinvar/
dbSNP 141, http://www.ncbi.nlm.nih.gov/projects/SNP/
Exome Aggregation Consortium (ExAC) Browser, http://exac.broadinstitute.org/
NHLBI Exome Sequencing Project (ESP) Exome Variant Server, http://evs.gs.washington.edu/EVS/
OMIM, http://www.omim.org/
RefSeq, http://www.ncbi.nlm.nih.gov/refseq/
Residual Variation Intolerance Score (RVIS), http://genic-intolerance.org
SeattleSeq Variation Annotation, http://snp.gs.washington.edu/SeattleSeqAnnotation138/
UCSC Genome Browser, http://genome.ucsc.edu
World Health Organization Child Growth Standards, http://www.who.int/childgrowth/standards/en/

References

1. Gilmore, E.C., and Walsh, C.A. (2013). Genetic causes of microcephaly and lessons for neuronal development. Wiley Interdiscip. Rev. Dev. Biol. *2*, 461–478.
2. Paridaen, J.T., and Huttner, W.B. (2014). Neurogenesis during development of the vertebrate central nervous system. EMBO Rep. *15*, 351–364.
3. Bond, J., Roberts, E., Mochida, G.H., Hampshire, D.J., Scott, S., Askham, J.M., Springell, K., Mahadevan, M., Crow, Y.J., Markham, A.F., et al. (2002). ASPM is a major determinant of cerebral cortical size. Nat. Genet. *32*, 316–320.
4. Bond, J., Roberts, E., Springell, K., Lizarraga, S.B., Scott, S., Higgins, J., Hampshire, D.J., Morrison, E.E., Leal, G.F., Silva, E.O., et al. (2005). A centrosomal mechanism involving CDK5RAP2 and CENPJ controls brain size. Nat. Genet. *37*, 353–355.
5. Kumar, A., Girimaji, S.C., Duvvari, M.R., and Blanton, S.H. (2009). Mutations in STIL, encoding a pericentriolar and centrosomal protein, cause primary microcephaly. Am. J. Hum. Genet. *84*, 286–290.
6. Bilgüvar, K., Oztürk, A.K., Louvi, A., Kwan, K.Y., Choi, M., Tatli, B., Yalnizoğlu, D., Tüysüz, B., Cağlayan, A.O., Gökben,

S., et al. (2010). Whole-exome sequencing identifies recessive WDR62 mutations in severe brain malformations. Nature *467*, 207–210.
7. Guernsey, D.L., Jiang, H., Hussin, J., Arnold, M., Bouyakdan, K., Perry, S., Babineau-Sturk, T., Beis, J., Dumas, N., Evans, S.C., et al. (2010). Mutations in centrosomal protein CEP152 in primary microcephaly families linked to MCPH4. Am. J. Hum. Genet. *87*, 40–51.
8. Nicholas, A.K., Khurshid, M., Désir, J., Carvalho, O.P., Cox, J.J., Thornton, G., Kausar, R., Ansar, M., Ahmad, W., Verloes, A., et al. (2010). WDR62 is associated with the spindle pole and is mutated in human microcephaly. Nat. Genet. *42*, 1010–1014.
9. Gauthier-Fisher, A., Lin, D.C., Greeve, M., Kaplan, D.R., Rottapel, R., and Miller, F.D. (2009). Lfc and Tctex-1 regulate the genesis of neurons from cortical precursor cells. Nat. Neurosci. *12*, 735–744.
10. Sarkisian, M.R., Li, W., Di Cunto, F., D'Mello, S.R., and LoTurco, J.J. (2002). Citron-kinase, a protein essential to cytokinesis in neuronal progenitors, is deleted in the flathead mutant rat. J. Neurosci. *22*, RC217.
11. Di Cunto, F., Imarisio, S., Hirsch, E., Broccoli, V., Bulfone, A., Migheli, A., Atzori, C., Turco, E., Triolo, R., Dotto, G.P., et al. (2000). Defective neurogenesis in citron kinase knockout mice by altered cytokinesis and massive apoptosis. Neuron *28*, 115–127.
12. El Amine, N., Kechad, A., Jananji, S., and Hickson, G.R. (2013). Opposing actions of septins and Sticky on Anillin promote the transition from contractile to midbody ring. J. Cell Biol. *203*, 487–504.
13. Green, R.A., Paluch, E., and Oegema, K. (2012). Cytokinesis in animal cells. Annu. Rev. Cell Dev. Biol. *28*, 29–58.
14. Gai, M., Camera, P., Dema, A., Bianchi, F., Berto, G., Scarpa, E., Germena, G., and Di Cunto, F. (2011). Citron kinase controls abscission through RhoA and anillin. Mol. Biol. Cell *22*, 3768–3778.
15. Bassi, Z.I., Verbrugghe, K.J., Capalbo, L., Gregory, S., Montembault, E., Glover, D.M., and D'Avino, P.P. (2011). Sticky/Citron kinase maintains proper RhoA localization at the cleavage site during cytokinesis. J. Cell Biol. *195*, 595–603.
16. Ackman, J.B., Ramos, R.L., Sarkisian, M.R., and Loturco, J.J. (2007). Citron kinase is required for postnatal neurogenesis in the hippocampus. Dev. Neurosci. *29*, 113–123.
17. Li, R., Li, Y., Fang, X., Yang, H., Wang, J., Kristiansen, K., and Wang, J. (2009). SNP detection for massively parallel whole-genome resequencing. Genome Res. *19*, 1124–1132.
18. Li, R., Yu, C., Li, Y., Lam, T.W., Yiu, S.M., Kristiansen, K., and Wang, J. (2009). SOAP2: an improved ultrafast tool for short read alignment. Bioinformatics *25*, 1966–1967.
19. Soukarieh, O., Gaildrat, P., Hamieh, M., Drouet, A., Baert-Desurmont, S., Frébourg, T., Tosi, M., and Martins, A. (2016). Exonic Splicing Mutations Are More Prevalent than Currently Estimated and Can Be Predicted by Using In Silico Tools. PLoS Genet. *12*, e1005756.
20. Gaildrat, P., Killian, A., Martins, A., Tournier, I., Frébourg, T., and Tosi, M. (2010). Use of splicing reporter minigene assay to evaluate the effect on splicing of unclassified genetic variants. Methods Mol. Biol. *653*, 249–257.
21. Abecasis, G.R., Altshuler, D., Auton, A., Brooks, L.D., Durbin, R.M., Gibbs, R.A., Hurles, M.E., and McVean, G.A.; 1000 Genomes Project Consortium (2010). A map of human genome variation from population-scale sequencing. Nature *467*, 1061–1073.
22. Psaty, B.M., O'Donnell, C.J., Gudnason, V., Lunetta, K.L., Folsom, A.R., Rotter, J.I., Uitterlinden, A.G., Harris, T.B., Witteman, J.C., and Boerwinkle, E.; CHARGE Consortium (2009). Cohorts for Heart and Aging Research in Genomic Epidemiology (CHARGE) Consortium: Design of prospective meta-analyses of genome-wide association studies from 5 cohorts. Circ Cardiovasc Genet *2*, 73–80.
23. Lek, M., Karczewski, K., Minikel, E., Samocha, K., Banks, E., Fennell, T., O'Donnell-Luria, A., Ware, J., Hill, A., Cummings, B., et al. (2015). Analysis of protein-coding genetic variation in 60,706 humans. bioRxiv http://dx.doi.org/10.1101/030338.
24. Cooper, G.M., Stone, E.A., Asimenos, G., Green, E.D., Batzoglou, S., and Sidow, A.; NISC Comparative Sequencing Program (2005). Distribution and intensity of constraint in mammalian genomic sequence. Genome Res. *15*, 901–913.
25. Kircher, M., Witten, D.M., Jain, P., O'Roak, B.J., Cooper, G.M., and Shendure, J. (2014). A general framework for estimating the relative pathogenicity of human genetic variants. Nat. Genet. *46*, 310–315.
26. Petrovski, S., Wang, Q., Heinzen, E.L., Allen, A.S., and Goldstein, D.B. (2013). Genic intolerance to functional variation and the interpretation of personal genomes. PLoS Genet. *9*, e1003709.
27. Gleeson, J.G., Allen, K.M., Fox, J.W., Lamperti, E.D., Berkovic, S., Scheffer, I., Cooper, E.C., Dobyns, W.B., Minnerath, S.R., Ross, M.E., and Walsh, C.A. (1998). Doublecortin, a brain-specific gene mutated in human X-linked lissencephaly and double cortex syndrome, encodes a putative signaling protein. Cell *92*, 63–72.
28. Fry, A.E., Cushion, T.D., and Pilz, D.T. (2014). The genetics of lissencephaly. Am. J. Med. Genet. C. Semin. Med. Genet. *166C*, 198–210.
29. Moon, H.M., and Wynshaw-Boris, A. (2013). Cytoskeleton in action: lissencephaly, a neuronal migration disorder. Wiley Interdiscip. Rev. Dev. Biol. *2*, 229–245.
30. Li, H., Bielas, S.L., Zaki, M.S., Ismail, S., Farfara, D., Um, K., Rosti, R.O., Scott, E.C., Tu, S., Chi, N.C., et al. (2016). Biallelic Mutations in Citron Kinase Link Mitotic Cytokinesis to Human Primary Microcephaly. Am. J. Hum. Genet. *99*, this issue, 501–510.
31. Morris-Rosendahl, D.J., and Kaindl, A.M. (2015). What next-generation sequencing (NGS) technology has enabled us to learn about primary autosomal recessive microcephaly (MCPH). Mol. Cell. Probes *29*, 271–281.
32. Higgins, J., Midgley, C., Bergh, A.M., Bell, S.M., Askham, J.M., Roberts, E., Binns, R.K., Sharif, S.M., Bennett, C., Glover, D.M., et al. (2010). Human ASPM participates in spindle organisation, spindle orientation and cytokinesis. BMC Cell Biol. *11*, 85.
33. Pulvers, J.N., Bryk, J., Fish, J.L., Wilsch-Bräuninger, M., Arai, Y., Schreier, D., Naumann, R., Helppi, J., Habermann, B., Vogt, J., et al. (2010). Mutations in mouse Aspm (abnormal spindle-like microcephaly associated) cause not only microcephaly but also major defects in the germline. Proc. Natl. Acad. Sci. USA *107*, 16595–16600.
34. Paramasivam, M., Chang, Y.J., and LoTurco, J.J. (2007). ASPM and citron kinase co-localize to the midbody ring during cytokinesis. Cell Cycle *6*, 1605–1612.
35. Roberts, M.R., Bittman, K., Li, W.W., French, R., Mitchell, B., LoTurco, J.J., and D'Mello, S.R. (2000). The flathead mutation causes CNS-specific developmental abnormalities and apoptosis. J. Neurosci. *20*, 2295–2306.
36. Epi4K Consortium (2012). Epi4K: gene discovery in 4,000 genomes. Epilepsia *53*, 1457–1467.

The American Journal of Human Genetics, Volume *99*

Supplemental Data

Mutations in Citron Kinase Cause Recessive Microlissencephaly with Multinucleated Neurons

Brian N. Harding, Amanda Moccia, Séverine Drunat, Omar Soukarieh, Hélène Tubeuf, Lyn S. Chitty, Alain Verloes, Pierre Gressens, Vincent El Ghouzzi, Sylvie Joriot, Ferdinando Di Cunto, Alexandra Martins, Sandrine Passemard, and Stephanie L. Bielas

Supplemental Data

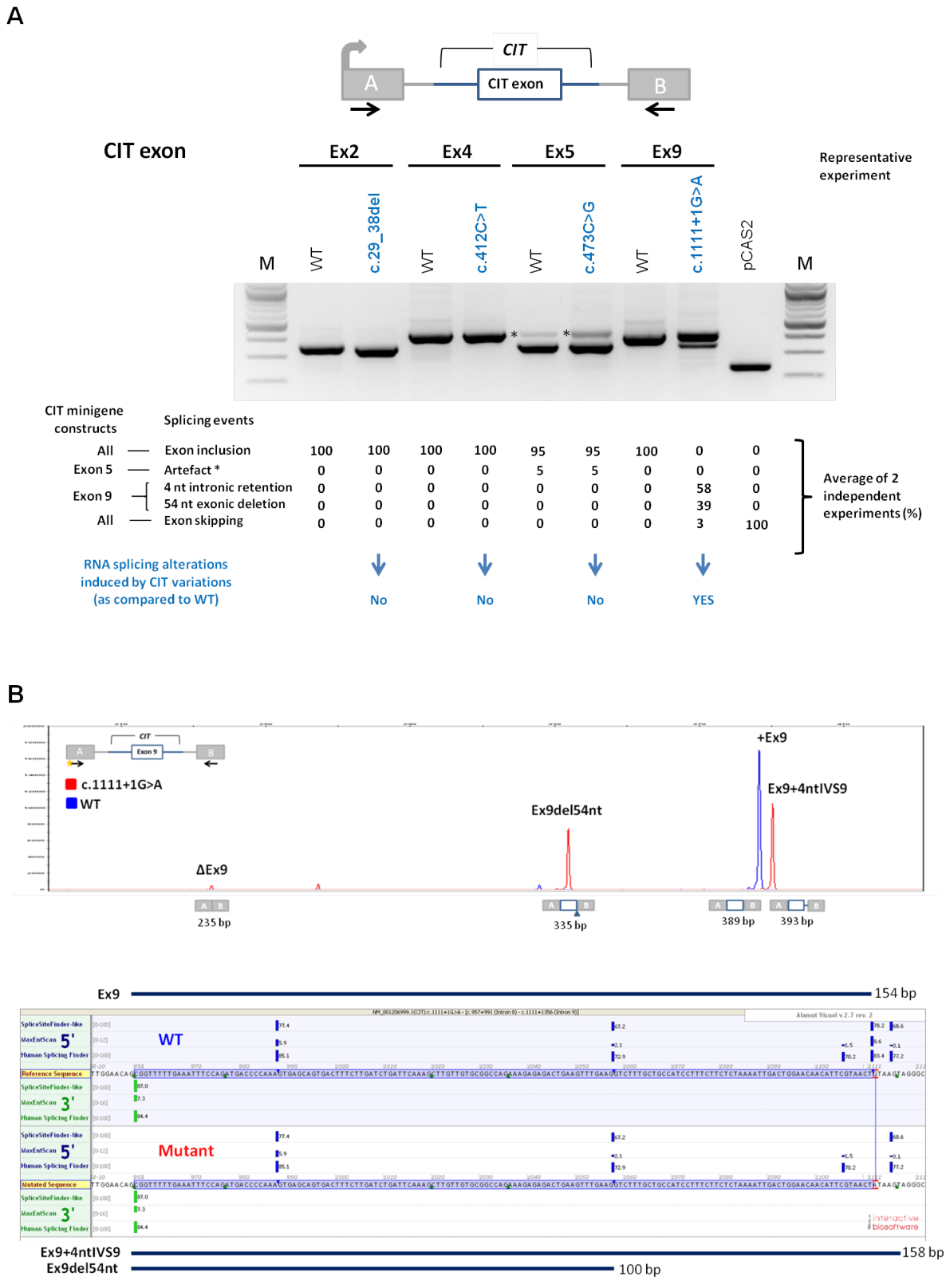

Figure S1. Detection of variant-induced *CIT* splicing alterations by using a minigene splicing assay. (A) Analysis of the splicing pattern of pCAS2 minigenes carrying *CIT* variants identified in microcephaly probands described in this study, as indicated. The top panel

represents the structure of pCAS2-CIT minigenes used in the minigene splicing assay. The grey arrow indicates the CMV promoter, boxes represent exons, lines in between indicate introns, and arrows below the exons represent primers used in RT-PCR reactions (Table S1). The minigenes were generated by inserting a genomic fragment containing the exon of interest and at least 150 nucleotides of the flanking introns into the intron of pCAS2, as described in Gaildrat et al. (either by using proband gDNA as template or by introducing the variants into the minigenes by site-directed mutagenesis)[1]. Then, wild-type (WT) and mutant constructs, as indicated, were transfected into HeLa cells and the minigenes' transcripts were analyzed by RT-PCR 24 hours later. The image shows the results of a representative experiment in which the RT-PCR products were separated on a 2.5% agarose gel stained with ethidium bromide and visualized by exposure to ultraviolet light. M indicates a 100 bp DNA ladder (New England Biolabs). The splicing events indicated under the gel are based on equivalent RT-PCR reactions performed by using a fluorescent forward primer (Table S1) and then separated in denaturing conditions by capillary electrophoresis on an automated sequencer (Applied Biosystems). Quantification results were obtained by using the GeneMapper v5.0 software (Applied Biosystems) and correspond to the average of two fluorescent-RT-PCR independent experiments. (B) Representative fluorescent RT-PCR experiment using pCAS2-*CIT* c.1111+1G>A-derived data as an example. The top panel shows superposed peaks corresponding to the WT and mutant products (in blue and red, respectively), as indicated. The bottom panel illustrates the outcome of the minigene assay relative to *CIT* exon 9 splicing both in the WT (top) and mutant (bottom) contexts, as well as *in silico* predictions relative to 5'ss and 3'ss in the genomic region of interest. *In silico* predictions were obtained by simultaneously interrogating 3 algorithms (SpliceSiteFinder-Like, MaxEntScan, and Human Splice Finder) through the integrated software tool Alamut (Interactive Biosoftware, France, http://www.interactive-biosoftware.com), as previously described[2]. For simplicity, thresholds for 5'ss and 3'ss scores were set at 66 and 84 for SpliceSiteFinder-Like, 0 and 7 for MaxEntScan, and at 70 and 84 for Human Splice Finder, respectively.

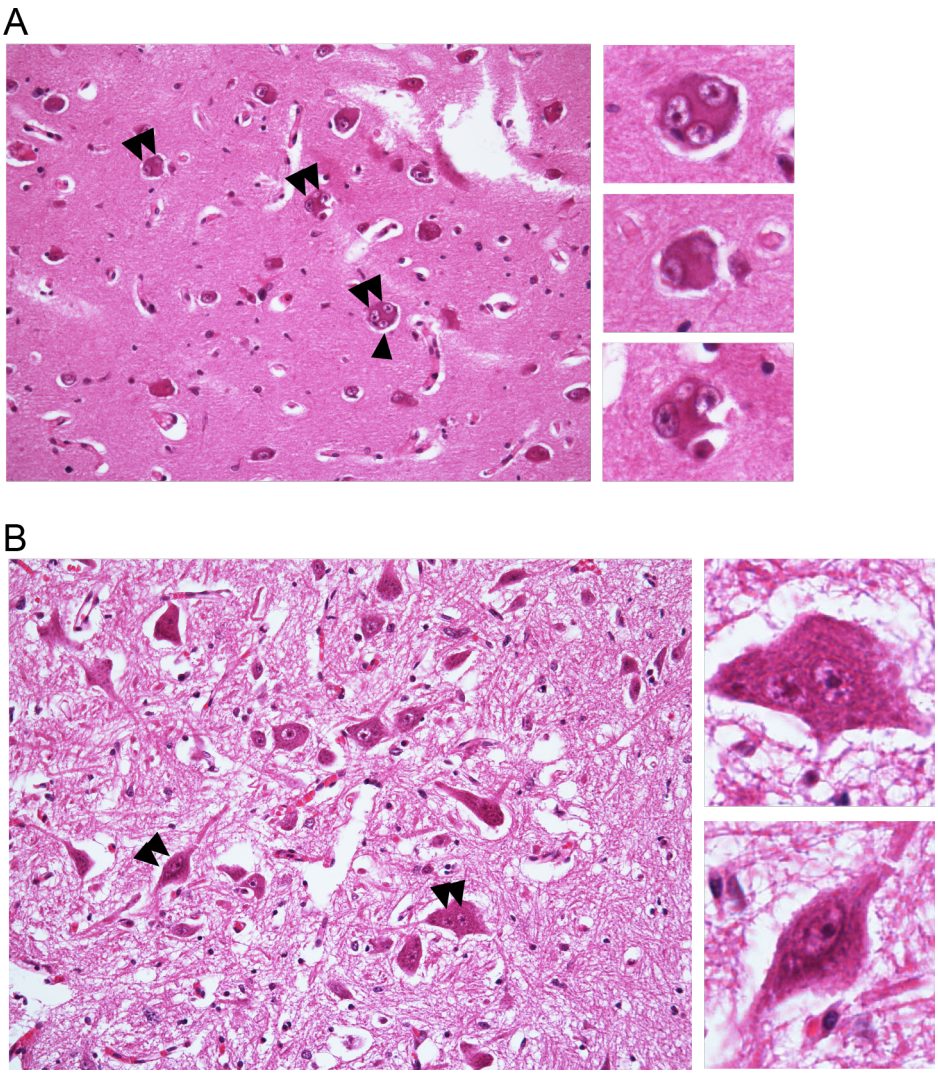

Figure S2. Multinucleated neurons throughout the neuraxis of Proband B. (**A**) Thalamus, (**B**) Spinal cord anterior horn. Cells indicated by arrowheads are enlarged in the inserts and multinucleated.

Table S1. Primers used in the pCAS2 minigene splicing assay for the analysis of *CIT* variations in exons 2, 4, 5 and 9.

Purpose	Forward (F) or reverse (R) primers	
	Name	Sequence (5'-3')
PCR (cloning/minigene preparation)	CIT_Ex2 InFus BamHI-F	AAGAAGTGCA*GGATCC*GTCAGATAAGTGTATCATCTCCTGTCA
	CIT_Ex2 InFus MluI-R	TCAAAACAAG*ACGCGT*TTCCCCTAAAATATTATCCCTGGTCC
	CIT_Ex4 InFus BamHI-F	AAGAAGTGCA*GGATCC*GTAGCTGCCATGGAAACTGTAC
	CIT_Ex4 InFus MluI-R	TCAAAACAAG*ACGCGT*CATCAAGAGGAATTTGTGAGCCTTC
	CIT_Ex5 InFus BamHI-F	AAGAAGTGCA*GGATCC*GGCTAAGTGACAGCCCCTTC
	CIT_Ex5 InFus MluI-R	TCAAAACAAG*ACGCGT*ACCACGTTCAGCCCAATGAG
	CIT.ex9.BamHI-F	TGGGAA*GGATCC*TTTGGTCCAAAGGGAAGAGGG
	CIT.ex9.MluI-R	ACTCAA*ACGCGT*CTACATCATTAGCCTTTACTACTCCTGTAG
Sequencing of minigene inserts	pCAS-Seq-F	GGGTCAATAGCAGTGAGAGG
	pCAS-Seq-R	GCTCCATTTCACAGGTAGAGA
Site-directed mutagenesis by two-stage overlap PCR	CIT Ex2 c.29_38del-F	ATATGGAGCGCGGA*TGCTGGTGCTGCTG*
	CIT Ex2 c.29_38del-R	CAGCAGCACCAGCA*TCCGCGCTCCATAT*
	CIT Ex4 c.412CT-F	GGCCCAGGAGTAGGTAGGAGG
	CIT Ex4 c.412CT-R	CCTCCTACCTACTCCTGGGCC
	CIT Ex5 c.473CG-F	GCCCGTGGATCCGCCAATTACAG
	CIT Ex5 c.473CG-R	CTGTAATTGGCGGATCCACGGGC
RT-PCR and sequencing of RT-PCR products	pCAS-KO1-F	TGACGTCGCCGCCCATCAC
	pCAS-2R	ATTGGTTGTTGAGTTGGTTGTC
Fluorescent RT-PCR	6FAM-pCAS-KO1-F	TGACGTCGCCGCCCATCAC
	pCAS-2R	ATTGGTTGTTGAGTTGGTTGTC

Table S2. Mammalian models of null mutations in *CIT.*

Species	**Human Proband B**	***Cit*$^{-/-}$ Knockout Mouse[3] (Di Cunto et al. 2000)**	***Flathead fh/fh* Mutant Rat[4,5] (Sarkisian et al. 2002) (Ackman et al. 2007)**
***Citron Kinase* Mutation**	10 bp deletion in exon 2	Conditional excision exon 2 by *Cre* mediated homologous recombination	Spontaneous 1 bp deletion in exon 1
Predicted Mutational Impact	Frameshift causing a premature stop codon 25 amino acids from start site	Premature stop codon	Frameshift causing a premature stop codon 27 amino acids from start site
***CIT* Transcript**	Predicted NMD	NMD	NMD
Brain Size and Weight	Microcephalic and ~1/10 of the brain weight of an average newborn	Microcephalic 50% brain weight reduction	Microcephalic 50% brain size reduction
Cerebral Cortex Abnormalities	Cortex shows cytological and organizational abnormalities. Six layer arrangement replaced by a molecular layer and two broad layers. Presence of multinucleated neurons.	40% reduction in cerebral cortex thickness. Disorganized lamination of 6-layer cortex. Presence of binucleated cells.	Neocortex displays a reduced number of neurons but normal lamination. Presence of binucleated neurons in neocortex.
Cerebellar Abnormalities	Hypoplastic and dysplastic cerebellar cortex, and disrupted laminar architecture. Crowded layer of Purkinje cells with simple dendritic arborizations. Binucleated Purkinje cells and granule cells.	70% cerebellum size reduction. Crowded layer of Purkinje cells with simple dendritic arborizations. Presence of binucleated cells.	Cerebellum displays a reduced number of neurons. Presence of binucleated neurons.
Hippocampal Abnormalities	Small and disorganized Ammon's horns. Only a small remnant of dentate fascia. Binucleated granule cells.	Normal Ammon's horn cell density and lamination. Essentially absent dentate gyrus.	Dentate gyrus displays a reduced number of neurons. Presence of binucleated neurons.
Additional Locations of Multinucleated Cells	Thalamus, striatum, pallidum, brain stem, spinal cord and PNS	Thalamus	Striatum, thalamus, midbrain, hindbrain, and spinal cord
Other Phenotypic Abnormalities	Kidney and heart defects, facial dysmorphisms, and rotated lower limbs	Ataxia, seizures, and failure to thrive	Seizures and disrupted development of the retina

NMD = Nonsense mediated decay, PNS = Peripheral Nervous System

Table S3. Presence of binucleated neurons by neuroanatomic area.

Presence of binucleated neurons by anatomic area	
neocortex	
hippocampus (pyramidal and granule cells)	
thalamus	
striatum (large and small cells)	
pallidum	
cerebellum	cerebellar cortex (Purkinje and granule cells)
	dentate nucleus
brain stem	midbrain tectum
	oculomotor nuclei
	pontine reticular formation
	nuclei pontis
	abducens nucleus
	inferior olive
	red nucleus
spinal cord & PNS	anterior horn
	autonomic ganglion

PNS = Peripheral nervous system

Supplemental References

1. Gaildrat, P., Killian, A., Martins, A., Tournier, I., Frébourg, T., and Tosi, M. (2010). Use of splicing reporter minigene assay to evaluate the effect on splicing of unclassified genetic variants. Methods Mol Biol 653, 249-257.

2. Soukarieh, O., Gaildrat, P., Hamieh, M., Drouet, A., Baert-Desurmont, S., Frébourg, T., Tosi, M., and Martins, A. (2016). Exonic Splicing Mutations Are More Prevalent than Currently Estimated and Can Be Predicted by Using In Silico Tools. PLoS Genet 12, e1005756.

3. Di Cunto, F., Imarisio, S., Hirsch, E., Broccoli, V., Bulfone, A., Migheli, A., Atzori, C., Turco, E., Triolo, R., Dotto, G.P., et al. (2000). Defective neurogenesis in citron kinase knockout mice by altered cytokinesis and massive apoptosis. Neuron 28, 115-127.

4. Sarkisian, M.R., Li, W., Di Cunto, F., D'Mello, S.R., and LoTurco, J.J. (2002). Citron-kinase, a protein essential to cytokinesis in neuronal progenitors, is deleted in the flathead mutant rat. J Neurosci 22, RC217.

5. Ackman, J.B., Ramos, R.L., Sarkisian, M.R., and Loturco, J.J. (2007). Citron kinase is required for postnatal neurogenesis in the hippocampus. Dev Neurosci 29, 113-123.